Chimica Techno Acta
published by Ural Federal University
eISSN 2411-1414
chimicatechnoacta.ru

LETTER
2024, vol. 11(4), No. 202411417
DOI: 10.15826/chimtech.2024.11.4.17

Ag-decorated hollow copper microtubes as a photocathode for the hydrogen evolution reaction

Dmitry S. Dmitriev *, Maksim I. Tenevich

Ioffe Institute, Saint-Petersburg 194021, Russia
* Corresponding author: elchemorg@gmail.com

This paper belongs to a Regular Issue.

Abstract

This paper presents the results of a photoelectrocatalytic study for a copper-silver system obtained in the form of microtubes using electrochemical template synthesis. CuO_x/Cu hollow microtubes (HT) decorated with nanoscale silver particles by electrodeposition demonstrate the cathode photocurrent in 7.6 uAcm^{-2} when using LED light sources in the UVA-Vis spectral region and low polarization values. It was shown that the highest intensity of the photoresponse is achieved in the visible region at a wavelength of 450 nm. The stability test suggests that the retention of Ag/CuO_x-HT is 95% after 12 hours of functioning.

Keywords

photocathode
hollow microtubes
copper
template synthesis
hydrogen evolution reaction

Received: 11.10.24
Revised: 18.11.24
Accepted: 20.11.24
Available online: 25.11.24

Supplementary materials

1. Introduction

Considering hydrogen as a fuel for the energy industry of the future, one of the main tasks is to efficiently, eco-friendly and economically produce it by various physico-chemical methods. Electrocatalytic and photocatalytic methods are deemed to be the most promising. In the framework of these techniques, electrode and photoactive materials are being developed that can reduce the economic and energy costs of hydrogen production. Many works have been devoted to the research of oxide and metal oxide systems as photoelectrode materials for water splitting. These works are mainly dedicated to photoanodes based on titanium, zinc, and cadmium oxides [1–5] and photocathodes based on copper oxides [6–10]. An important aspect in the development of materials for photoelectrocatalysis is the surface area of the catalyst and the presence of potentially active reaction centers on it. In the synthesis of electrode materials, it makes sense to aspire to 2D and 3D structures enhanced by nanocrystalline defects that can act as active centers [11-15]. The authors of [13] report the fabrication of a flexible and photosensitive electrode for electrocatalysis using efficient, robust, and photosensitive two-dimensional molybdenum disulfide (2D-MoS_2) nanosheets and flexible, lightweight, large area, and conducting Ag metal coated cellulose paper. The MoS_2/Ag cathode shows enhanced hydrogen evolution reaction activity under visible light and facilitates a faster catalytic reaction.

Doping of the photoactive matrix with noble metals is practiced as a way to improve the catalytic properties of electrode materials. Recently, the addition of gold and/or silver particles has been used for photocathodes based on copper oxides. It was noted [16–24] that Ag-doping results in minimal changes to the bandgap and bandgap energies. Improved conductivity and photoresponse (up to 4 times) compared to undoped samples were recorded. A high dopant concentration reduces performance due to recombination centers, which inhibit the increased charge-separation efficiency. Au was also found to reduce the recombination phenomenon. Computational studies indicate that the electronic structure of Au-doped Cu_2O is affected in a manner almost identical to that observed for Ag.

This study is a logical continuation of the work published previously [25]. Modification of the surface of copper microtubes with silver particles has improved the electrochemical characteristics of the material when functioning as a photocathode in a water splitting reaction. In this paper, we demonstrate for the first time the possibility of using electrochemical template synthesis as a method for producing photoactive electrode materials suitable for the process of water splitting, with a particular focus on hydrogen production.

2. Experimental

2.1. Synthesis of Ag/CuO_x - HT

Hollow copper microtubules, produced by the electrochemical template synthesis technique described in the paper [25] were used as a precursor in this study. Microtubes with copper oxides were decorated by silver particles via electrodeposition. A solution of silver sulfosalicylic complex was used as an electrolyte (Table S1). The anodes were silver plates. The process was performed at a current density of 5 $mAcm^{-2}$ for 1 min using a magnetic stirrer. Next, two-step rinsing was executed in warm (60 °C) and room-temperature (25 °C) distillate followed by drying at 105 °C for 1 h. The hollow tube samples before and after modification were labeled as CuO_x-HT and Ag/CuO_x-HT. The experimental procedure is illustrated in Figure S1.

2.2. Characterization methods

The structure and morphology of the synthesized samples were studied using a scanning electron microscope TESCAN SEM with the VEGA 3 SBH microanalyzer (EDX-mapping). The SEM measurements were carried out at an operating voltage of 30 kV, with magnification up to 40kx. The EDX test was fulfilled at a similar operating voltage in the energy range of 10 keV with 2048 operating channels and a data accumulation time of 2500 seconds.

XRD analysis was performed on powdered samples using the Bruker D2 Phaser instrument base. The measurement was carried out on a cobalt tube (Co Kα radiation, λ = 0.17889 nm), accelerating voltage 30 kV, current 10 mA, angle range 10–60°, step 0.01°, speed 2° per minute. For further analysis, the results were recalculated for the radiation of the copper tube (Cu Kα radiation, λ = 0.15405 nm). The diffractograms were processed using a pseudo Voigt profile. Quantitative analysis and calculation of the unit cell parameters were performed using the Rietveld method. The crystallite sizes were calculated according to the Scherrer equation.

The diffuse reflectance spectra (DRS) of the samples were obtained using an Avaspec-ULS2048 spectrophotometer equipped with an AvaSphere-30 integrating sphere in the range of 300–800 nm. The bandgap energy (E_g) was defined using a plot in Tauc coordinates ($[F(R)h\nu]^n$ – $h\nu$) using the Kubelka-Munk function.

2.3. Photoelectrochemical testing

The photoelectrochemical (PEC) performances of the synthesized materials were tested by voltammetry and electrochemical impedance spectroscopy in dark/irradiation mode using an Elins P-45X galvanostat-potentiostat with iR compensation. A Pt plate and AgCl/Ag ($E^o_{AgCl/Ag}$ = 0.197 V) were used as a counter electrode and a reference electrode, respectively. The solution of 0.5 M Na_2SO_4 (pH = 7) acted as an electrolyte in all electrochemical measurements. The light sources used were 3 W LEDs with wavelengths of 365, 450, 525, 570 nm, as well as a Uniel A60-9W-UVAD LED lamp with a maximum intensity at a wavelength of 410 nm.

The working electrode was fabricated by applying a suspension of the active material with a binder (LIQUION LQ-1115) to ITO-glass in a ratio of 1 mg per 40 μL. To form a stable suspension, we performed ultrasonic treatment for 20 min and stirring on a Vortex mixer immediately before application to ITO-glass. Ultrasonic treatment in ethanol for 5 min was used as a preliminary preparation of ITO-glass. The suspension applied to ITO-glass (V = 40 μL) was dried using a laboratory heating plate for 5 min. The selection of ITO glass as a substrate for photoelectrochemical testing is due to its higher electrical conductivity compared to FTO and AZO materials

Voltammetry was performed in the potential range from −0.8 to 0.1 V vs AgCl/Ag with a sweep rate of 10 mVs^{-1}. For the impedance measurement, the alternating current signal with a bias of −0.65 V vs AgCl/Ag and an amplitude of 5 mV with a frequency ranging from 1 mHz to 1 MHz was applied to the electrochemical cell. The results of impedance measurements were processed in the EIS Spectrum Analyzer software. Voltammetric and impedance measurements were executed with and without irradiation by 9W Uniel-UVA lamp. The photoresponse was measured at a bias of −0.65 V vs AgCl/Ag and using LEDs with the abovementioned wavelengths. The photocurrent stability test was performed in potentiostatic mode at a bias of −0.65 V vs AgCl/Ag and using 9 W Uniel-UVA lamp for 12 h.

To determine the flatband potential (E_{fb}), the Mott-Schottky plot in coordinates $1/C^2 - E$ vs RHE was used at the intersection point with X-axis at frequency of 1000 Hz in the potential range from 0 to 1.5 V vs AgCl/Ag. The measurements were carried out in the dark mode. For the Mott-Schottky plot, the expression was used

$$\frac{1}{C^2} = (2\pi \cdot f \cdot Im)^2, \quad (1)$$

where f is the signal frequency, Hz, and Im is the imaginary component of the impedance hodograph, Ohm.

To convert the potential from the AgCl/Ag scale of the electrode to the reversible hydrogen electrode (RHE) scale, the formula was used:

$$E \text{ vs RHE} = E_{AgCl/Ag} + 0.197 + 0.0591\text{pH}. \quad (2)$$

The photoresponse was calculated as the current difference during irradiation and without it according to the expression

$$I_{ph} = I_{light} - I_{dark}. \quad (3)$$

The photocurrent density was calculated using the photocurrent value and the visible surface area of the ITO-coated substrate, which was equal to 1 cm^2:

$$j_{ph} = \frac{I_{ph}}{S}. \quad (4)$$

 DOI: 10.15826/chimtech.2024.11.4.17

3. Results and Discussion

Figure 1 shows the results of a study of the morphology and chemical composition in the surface of copper microtubes before and after modification by silver nanoparticles. During the electrodeposition of silver, the morphology of microtubes changes. A decrease in the wall thickness of microtubes is observed due to electrolytic cementation reactions ($Cu^0 + 2Ag^+ = Cu^{2+} + 2Ag^0$) and chemical etching of copper in an ammonia buffer occurring in parallel with the main process. The wall thickness of the microtube decreases from 1 to 0.75 μm. The silver particles formed on the microtube surface have an average size of 600 nm.

According to the results of the EDX analysis (Figure S2), silver nanoparticles are evenly distributed over the microtube surface, and the presence of copper oxides formed due to side chemical reactions is also observed.

The XRD analysis results (Figure 2) allow us to clarify that the surface copper oxides are represented as cubic Cu_2O (Pn-3m) with characteristic intense peaks at angles of 36.44 and 42.33 degrees (ICSD 261853). In addition, the XRD patterns show the presence of two metallic phases, Cu-cubic (Fm-3m) and Ag-cubic (Fm-3m). The Cu-cubic phase has characteristic peaks at 43.3 and 50.43 (ICSD 426938), and Ag-cubic at 38.11 and 44.3 (ICSD 181730) degrees, respectively.

The calculation of the phase content in the sample demonstrates values consistent with the data obtained by EDX and SEM methods. In particular, the redistribution of copper from metallic to oxide form is observed, and the mass content of silver , according to the refinement results, ranges from 15 to 7%. The results of the Rietveld refinement are presented in Table S2.

The average size of the copper crystallites in the 111 direction for the samples before and after modification is 28 and 23 nm, respectively. The formed silver nanoparticles have an average crystallite size of 21 nm. At the same time, the crystallinity index (I_c) decreases from 95 to 90%, which indicates the formation of an amorphous Cu_2O phase.

The formation of Cu_2O is due to the oxidation reaction of copper microtubes or the reduction of the passivation layer in the electrolytes used for electroreduction and silver plating. In both cases, the media used is alkaline (pH > 9), which causes reactions:

$$2Cu + 2OH^- = Cu_2O + H_2O + 2e \quad (5)$$

for freshly recovered copper or

$$2Cu(OH)_2 + 2e = Cu_2O + H_2O + 2OH^- \quad (6)$$

for passivated copper surface in the process of silvering the surface of microtubes.

Figure S3a and Figure S3b show the results of spectroscopy for Ag/CuO_x-HT sample. The analysis of DRS demonstrates that the most light absorption occurs at a wavelength of 465 nm, which is consistent with the obtained bandgap energy from the Tauc plot equal to 2.38 eV.

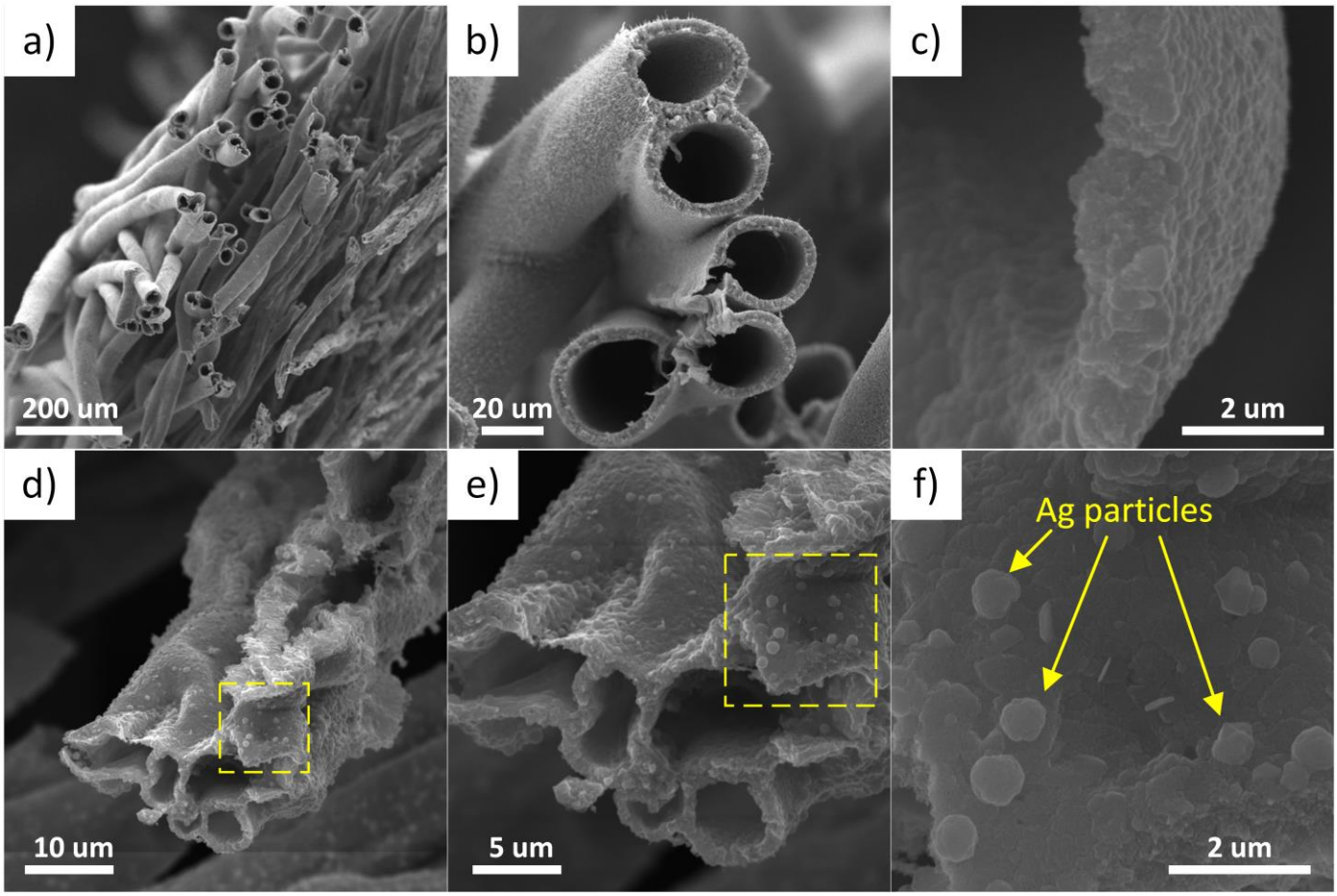

Figure 1 The SEM images of CuO_x-HT (a–c) and Ag/CuO_x-HT (d–f).

 DOI: 10.15826/chimtech.2024.11.4.17

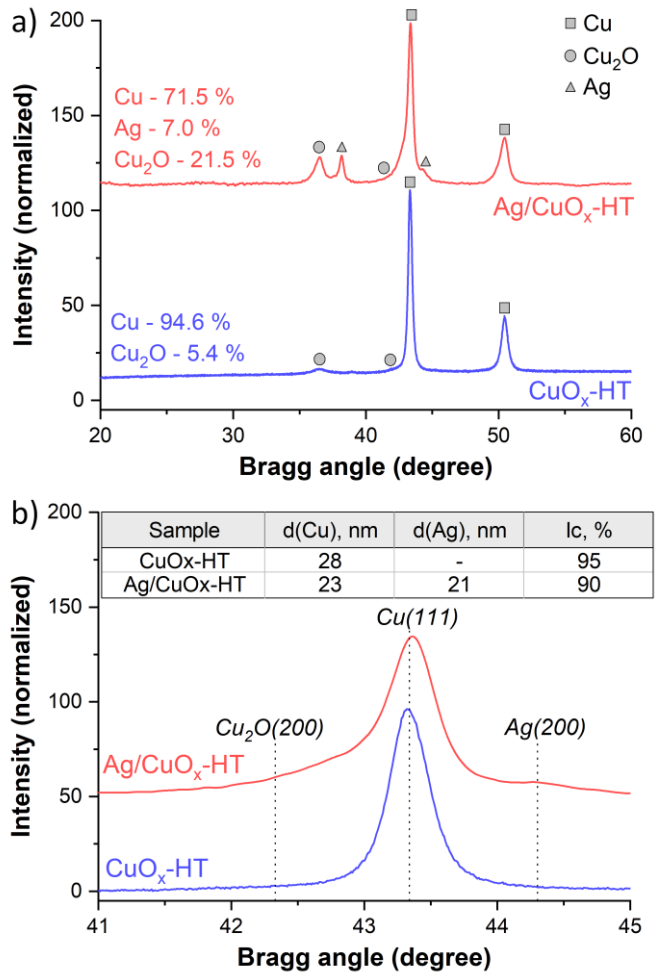

Figure 2 Survey (a) and comparative (b) XRD patterns of CuO_x-HT and Ag/CuO_x-HT samples.

In this case, the electronic transition is direct. The obtained value is confirmed by the results of other authors [26] and is mainly due to the presence of Cu_2O on the surface.

The analysis of the Mott-Schottky plot, combined with the results from the DRS, allows us to illustrate the photoelectrochemical reaction using an energy diagram. The negative slope of the plot (Figure S3c), in coordinates of $1/C^2$ – E vs RHE, indicates that Ag/CuO_x-HT is a p-type semiconductor. The flatband potential (E_{FB}), measured versus RHE, is 2.18 eV. For flatband of p-type semiconductors, this potential is near the position of the valence band (E_{VB}). Therefore, the position of the conduction band (E_{CB}) can be calculated using the following equation:

$$E_{CB} = E_{VB} - E_g \approx E_{FB} - E_g \quad (7)$$

and is equal to -0.2 eV (Figure S3d).

When a semiconductor and a metal particle come into contact, a Schottky barrier can form in the new material due to the different Fermi levels of Cu_2O and silver nanoparticles. Therefore, there is a rectification of charge carrier transfer, where the energetic difference at the interface between the semiconductor and metal drives electrons from the conduction band of Cu_2O into the silver nanoparticles. In the structure of Ag/CuO_x-HT, silver acts as an electron trap, minimizing the recombination of electron-hole pairs and improving photoelectrochemical efficiency.

The photoresponse of Ag/CuO_x-HT compared with CuO_x-HT (Figure S4) demonstrates an increase in photocurrent in the range of 365–570 nm with a maximum value difference of two times at a wavelength of 450 nm. Based on the results obtained, a more detailed study was carried out using a more powerful LED lamp with a characteristic wavelength of 410 nm.

Figures 3a and 3b present the chronoammetric plot and polarization curves for Ag/CuO_x-HT. It can be seen that with increasing lamp power the photoresponse rises, and in the stationary mode it is 7 uAcm^{-2}, while in the scanning mode is 7.2 uAcm^{-2} at 0 V vs RHE.

At the same time, there is a decrease in the absolute values of the Tafel slope and the exchange current density for the cathode process – the hydrogen evolution reaction (Figure 3c). The Tafel slope of 110 mVdec^{-1} corresponds to a reaction following the Volmer-Tafel mechanism:

$$M^* + H_2O + e \leftrightarrow MH_{ads} + OH^- \text{ (Volmer step)} \quad (8)$$

$$2MH_{ads} \leftrightarrow M^* + H_2 \text{ (Tafel step)} \quad (9)$$

An increase in the logarithm of the exchange current density from −5.3 to 5.0 indicates an improvement in the reaction kinetics during irradiation of the working electrode. The impedance spectra in Nyquist and Bode coordinates (Figure 3d and 3e) indicate a 1.5-fold decrease in the resistance of the electrode material (from 16 to 10 kOhm) when irradiated.

The stability test of the photoelectrode material under work conditions indicates that there is no degradation of the sample after 12 hours of operation with a nominal photocurrent density of 7.6 uAcm^{-2} (Figure 4a). The stability of the chemical composition and structure of the material was confirmed by the XRD results 95% (retention), which showed the presence of characteristic reflections before and after the test (Figure 4b).

Table S3 compares the results of this study to those of similar or related systems in other publications. The other researchers generally use more powerful light sources, such as full-spectrum xenon lamps with a power of 300 W. In this context, the results obtained with 3-9 W LED lamps provide information about the potential of using Ag/CuO_x-HT.

4. Limitations

When performing this study, optimization of the conditions for decorating copper microtubes with silver particles was not carried out. A detailed analysis of PEC properties has not been performed yet. These limitations will be eliminated with further research in the following publications.

 DOI: 10.15826/chimtech.2024.11.4.17

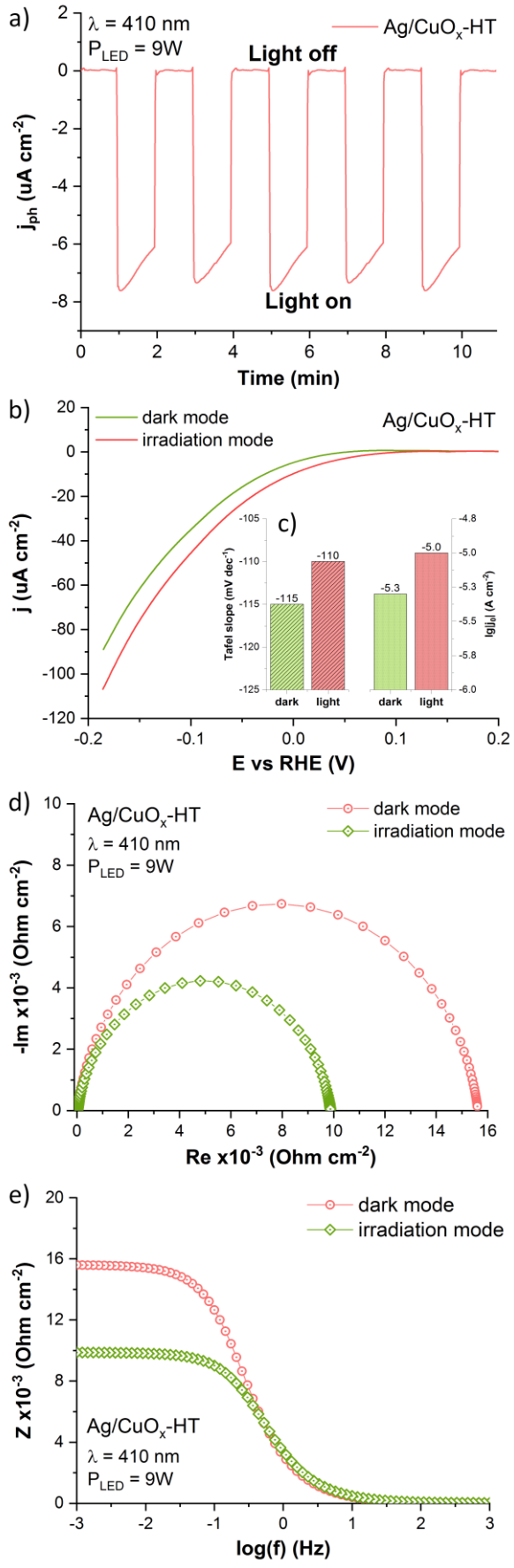

Figure 3 Photoelectrochemical performances of Ag/CuO_x-HT: stationary (On-Off) (a) and polarization (b) photocurrent curves, comparative bar of Tafel slope and exchange current density (c), Nyquist (d) and Bode (e) plot.

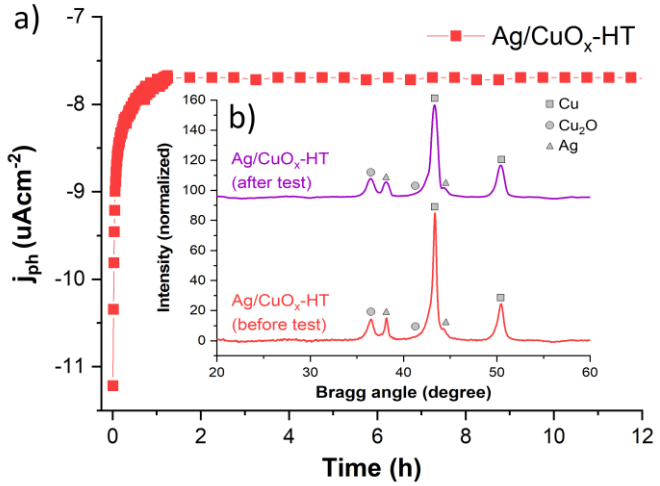

Figure 4 Photocurrent stability testing (a) and XRD patterns (b) before and after long-term tests.

5. Conclusions

The surface of copper microtubules was modified to improve photoelectrocatalytic properties by electrodeposition. It was shown that the presence of silver nanoparticles increases the photocurrent value by 2 times. The maximum value of the photoresponse was observed in the short-wavelength region of the visible spectrum of 400-450 nm. Long-term tests demonstrated the stability of the synthesized photocathode material.

• Supplementary materials

This manuscript contains supplementary materials, which are available on the corresponding online page.

• Funding

This research was supported by the State Assignment from the Ministry of Science and Higher Education of the Russian Federation for the Ioffe Institute of the Russian Academy of Sciences (project no. FFUG-2024-0036).

• Acknowledgments

SEM and EDX studies were performed using the analytical equipment of the Engineering Center of the St. Petersburg State Institute of Technology.

• Author contributions

Conceptualization: D.S.D.
Formal Analysis: D.S.D., M.I.T.
Investigation: D.S.D., M.I.T.
Methodology: D.S.D., M.I.T.
Supervision: D.S.D.
Validation: D.S.D., M.I.T.
Visualization: D.S.D.
Writing – original draft: D.S.D.
Writing – review & editing: D.S.D.

 DOI: 10.15826/chimtech.2024.11.4.17

• Conflict of interest

The authors declare no conflict of interest.

• Additional information

Author IDs:

Dmitry S. Dmitriev, Scopus ID 57192430838;
Maksim I. Tenevich, Scopus ID 57220137800.

Website:

Ioffe Institute, https://www.ioffe.ru/ru/.

References

1. Khusnun NF, Arshad A, Jalil AA, Firmansyah L, Hassan NS, Nabgan W, et al. An avant-garde of carbon-doped photoanode materials on photo-electrochemical water splitting performance: A review. J Electroanal Chem. 2023;929:117139. doi:10.1016/j.jelechem.2022.117139
2. Sawal MH, Jalil AA, Khusnun NF, Hassan NS, Bahari MB. A review of recent modification strategies of TiO_2-based photoanodes for efficient photoelectrochemical water splitting performance. Electrochim Acta. 2023;467:143142. doi:10.1016/j.electacta.2023.143142
3. Goktas S, Goktas A. A comparative study on recent progress in efficient ZnO based nanocomposite and heterojunction photocatalysts: A review. J Alloys Compd. 2021;863:158734. doi:10.1016/j.jallcom.2021.158734
4. Mohammadnezhad G, Momeni MM, Nasiriani F. Enhanced photoelectrochemical performance of tin oxide decorated tungsten oxide doped TiO2 nanotube by electrodeposition for water splitting. J Electroanal Chem. 2020;876:114505. doi:10.1016/j.jelechem.2020.114505
5. Momeni MM, Ghayeb Y, Davarzadeh M. Single-step electrochemical anodization for synthesis of hierarchical WO3-TiO2 nanotube arrays on titanium foil as a good photoanode for water splitting with visible light. J Electroanal Chem. 2015.739:149–55. doi:10.1016/j.jelechem.2014.12.030
6. Li C, He J, Xiao Y, Li Y, Delaunay J-J. Earth-abundant Cu-based metal oxide photocathodes for photoelectrochemical water splitting. Energy Environ Sci. 2020;13:3269–306. doi:10.1039/D0EE02397C
7. Chen P, Zhang P, Cui Y, Fu X, Wang Y. Recent progress in copper-based inorganic nanostructure photocatalysts: properties, synthesis and photocatalysis applications. Mater Today Sustain. 2023;21:100276. doi:10.1016/j.mtsust.2022.100276
8. Jeong D, Jo W, Jeong J, Kim T, Han S, Son M-K, et al. Characterization of Cu2O/CuO heterostructure photocathode by tailoring CuO thickness for photoelectrochemical water splitting. RSC Adv. 2022;12:2632–40. doi:10.1039/D1RA08863G
9. Son M-K. Key Strategies on Cu2O Photocathodes toward Practical Photoelectrochemical Water Splitting. Nanomaterials. 2023.13:3142. doi:10.3390/nano13243142
10. Guan L, Shu Y, Jiang Y, Zhao F, Wei Y, Yan J, et al. Rational design and fabrication of Cu_2O film as photoelectrode for water splitting. J Alloys Compd. 2023;956:170283. doi:10.1016/j.jallcom.2023.170283
11. Su Q, Zuo C, Liu M, Tai X. A Review on Cu2O-Based Composites in Photocatalysis: Synthesis, Modification, and Applications. Molecules. 2023;28:5576. doi:10.3390/molecules28145576
12. John S, Roy SC. CuO/Cu2O nanoflake/nanowire heterostructure photocathode with enhanced surface area for photoelectrochemical solar energy conversion. Appl Surf Sci. 2020;509:144703. doi:10.1016/j.apsusc.2019.144703
13. Pataniya PM, Sumesh C. Paper-Based Flexible and Photosensitive Electrodes for Electrochemical Hydrogen Evolution. ACS Appl Energy Mater. 2021;4:4815–22. doi:10.1021/acsaem.1c00377
14. Pataniya PM, Sumesh CK. Enhanced electrocatalytic hydrogen evolution reaction by injection of photogenerated electrons in Ag/WS2 nanohybrids. Appl Surf Sci. 2021;563:150323. doi:10.1016/j.apsusc.2021.150323
15. Markovskaya D V., Lomakina VA, Kozlova EA. Photoelectrochemical properties of Pt- and Ir-modified graphitic carbon nitride. Chim Techno Acta. 2024;11:1–10. doi:10.15826/chimtech.2024.11.2.08
16. Baran T, Visibile A, Busch M, He X, Wojtyla S, Rondinini S, et al. Copper Oxide-Based Photocatalysts and Photocathodes: Fundamentals and Recent Advances. Molecules. 2021;26:7271. doi:10.3390/molecules26237271
17. Uan J-Y, Chen Y-J, Hsu Y-H, Arpornwichanop A, Chen Y-S. Deposition of Li/Al layered double hydroxides on the graphite felts for the performance improvement of an all-vanadium redox flow battery. Mater Today Commun. 2021;27:102280. doi:10.1016/j.mtcomm.2021.102280
18. Bodhankar PM, Sarawade PB, Kumar P, Vinu A, Kulkarni AP, Lokhande CD, et al. Nanostructured Metal Phosphide Based Catalysts for Electrochemical Water Splitting: A Review. Small. 2022;18:2107572. doi:10.1002/smll.202107572
19. Polat K. A low cost flexible photocatalyst based on silver decorated Cu_2O nanowires. SN Appl Sci. 2020;2:1542. doi:10.1007/s42452-020-03354-1
20. Hu Y, Min X, Qi Y, Zhang W, Liu C, Wang Y, et al. Enhanced Photoelectrochemical Hydrogen Evolution on CuBi2O4 Photocathode with Silver as Conductive Channels. Catal Letters. 2024;154:34–41. doi:10.1007/s10562-023-04292-4
21. Xia Q, Liu X, Li H, Guan Y, Chen J, Chen Y, et al. Construction of the Z-scheme Cu2O-Ag/AgBr heterostructures to enhance the visible-light-driven photocatalytic water disinfection and antibacterial performance. J Alloys Compd. 2024;980:173665. doi:10.1016/j.jallcom.2024.173665
22. Lu W, Gu T, Jing X, Zhu Y, Yu L, Hou S, et al. Ag Nanoparticles-decorated p-type CuO/n-type ZnO heterojunction nanofibers with enhanced photocatalytic activities for dye degradation and disinfection. J Alloys Compd. 2023;968:171864. doi:10.1016/j.jallcom.2023.171864
23. Li Y, Luo K. Flexible cupric oxide photocathode with enhanced stability for renewable hydrogen energy production from solar water splitting. RSC Adv. 2019;9:8350–4. doi:10.1039/C9RA00865A
24. Park JE, Hu Y, Krizan JW, Gibson QD, Tayvah UT, Selloni A, et al. Stable Hydrogen Evolution from an AgRhO 2 Photocathode under Visible Light. Chem Mater. 2018;30:2574–82. doi:10.1021/acs.chemmater.7b04911
25. Dmitriev DS, Martinson KD, Popkov VI. Electrochemical template synthesis of copper hollow microtubes with dendritic surface and advanced HER performance. Mater Lett. 2021;305:130808. doi:10.1016/j.matlet.2021.130808
26. Yin T-H, Liu B-J, Lin Y-W, Li Y-S, Lai C-W, Lan Y-P, et al. Electrodeposition of Copper Oxides as Cost-Effective Heterojunction Photoelectrode Materials for Solar Water Splitting. Coatings. 2022;12:1839. doi:10.3390/coatings12121839

 DOI: 10.15826/chimtech.2024.11.4.17